5.2 Beamline Engineering

5.2.1 Introduction

The beamline engineering effort during the facility construction years focused on the design, construction, and commissioning of various beamline components, which included the beamline front ends, the experiment enclosures; various experiment-specific components, etc. These efforts have paid off as measured by the successful operation of user beamlines. During the past year, the focus of the staff working on the R&D in support of beamline engineering has moved to evaluation of the performance of beamline components, leading to new

concepts and developments for fututre beamlines. Attention was also given to the new requirements, present and future, to meet goals of the user scientific programs.

One of the major shortcomings in the manufacture of various beamline components by the vendors was their limited success in brazing Glidcopâ to various metals. The staff working on beamline engineering hence developed various brazing technologies and capabilities to bridge the gap so that users could successfully begin their scientific programs. In the next section, the brazing furnaces and their capabilities are described.

In order to meet new requirements of the users, conceptual and design changes in the front ends are needed in the newer beamlines planned for construction. These designs and their new capabilities are described in section 5.2.3.

Finally in section 5.2.4, a description of both a laser Doppler displacement meter and an angular encoder with sub-nanoradian sensitivity required for high-resolution monochromators is provided. These unique designs will have a much wider application in the future as users plan more sophisticated experiments.

5.2.2 Brazing Capabilities for Beamline Components

Small Brazing System

A new metallurgical brazing system has been developed by the Beamline Engineering Group that is used primarily for brazing small samples and heat transfer experimental tubes. Due to the small size of the system, it is ideal for brazing small components at a fraction of the cost compared to one of our larger brazing systems. The capability supports special needs of the users, as well as unique R&D needs for the beamline engineering effort. The small system size allows for rapid heating and cooling, and consequently samples can be processed in a minimal

amount of time. A Carbolite three-zone clam-shell-type resistance heating furnace is used as the heat source. The three zones are independently controllable via three temperature controllers remotely located on the system control module. A 2-inch (inside diameter) by 4-foot-long clear quartz tube equipped with quartz feedthrough end caps is used for the brazing chamber.

Vacuum Furnace for Large Component Brazing

Another brazing system has been developed to provide state-of-the-art brazing capabilities for future front-end and beamline components. This new system incorporates a significant number of improvements over our older system to provide several levels of automated control over the brazing process. As before, a thin-walled high-temperature material tube was used for the brazing chamber to minimize heating and cooling times, an essential requirement for brazing Glidcop®. A Hastolloy-X rolled and welded tube with a 7 1/2 inch inside diameter and 15 feet long was selected due to the superior high-temperature properties of this material. The long tube length provides the flexibility to braze very long parts.

A 15-kW three-zone Lindburg® clam-shell-type resistance heating furnace is used as the heat source and is mounted with precision slides on a rail system to allow easy movement of the furnace along the tube. The furnace is coupled via a magnet lock to a precision ball screw drive system, which is controllable from a remote keypad and joystick. The controller can be easily programmed from a PC to provide any combination of motion and positioning

referenced from a “home” position with a maximum speed of 2 inches per second. The motion control system provides the capability to oscillate the oven over long parts to achieve repeatable uniform heating and also provides an absolute position reference for repeating previous braze runs. The magnet lock can be instantly de-energized via a large emergency stop button to decouple the oven from the drive system.

As with the older brazing system, the three oven zones can be individually controlled from remote temperature controllers, however, an “auto-tune” feature has been added to eliminate the need to calibrate the braze run. Another key feature of the new system is a fully automated pump and purge controller. Prior to brazing, the chamber needs to be pumped and purged in a repetitive fashion with a high purity inert gas in order to “wash” contamination from the chamber walls and the component. If done manually, this process is time consuming. The pump and purge system will automatically perform this process, and the number of cycles and pumping times can be changed via keypads on the controller. The gas delivery system accommodates four separate gas sources, typically Ar, He, and two N_2 supplies. The microbleed circuit is used during the brazing process to achieve a reduced atmosphere in the chamber, and the quenching circuit is used to rapidly cool brazed parts. All of these circuits have precision flow-control valves and flow meters for repeatable gas delivery rates. The vacuum aspects of the new brazing system are far superior to the system used previously in this effort.

During the year, several braze techniques for joining stainless steel to GlidCop® were developed. These techniques were used to fabricate several fixed masks that are now installed in the front ends. In addition, some of the components for the SPring-8 front ends were designed and fabricated, which involved various specialized brazing jobs.

5-ID Ratchet-Wall Collimator Tube Examinations

In section 2.6.6, a detailed description of the sector 5 front-end problem was provided. This single incidence in which the ratchet-wall collimator was distorted required independent examination. The collimator, when isolated for study, showed considerable residual distortion.

The collimator itself was displaced by as much as 9 mm in the shield wall, with about a 6-mm bend in the tube. When it was examined in the laboratory, the residual bend was only 2.1 mm. In order to understand the source of this distortion, a detailed examination was performed. Corrosion was found in the lead shot surrounding the collimator. Chemical test results showed that most of the corrosion was aluminum oxide deposited on the lead shot. Lead oxides and concrete were also found, although the amounts were small in comparison.

A bend test was designed to simulate possible conditions in the shield wall. As shown in Fig. 5.11, approximately 36,000 N displaced the tube 7 mm and left a residual bend of 3.2 mm. In the actual front ends, the cause of such force is unclear; however, the pressure would not have been generated if both ends of the collimator were not clamped. As described in section 2.6.6, all ratchet-wall collimators were modified as a preventative measure to allow for changes in the collimator dimensions. The chemical

(a) (b)

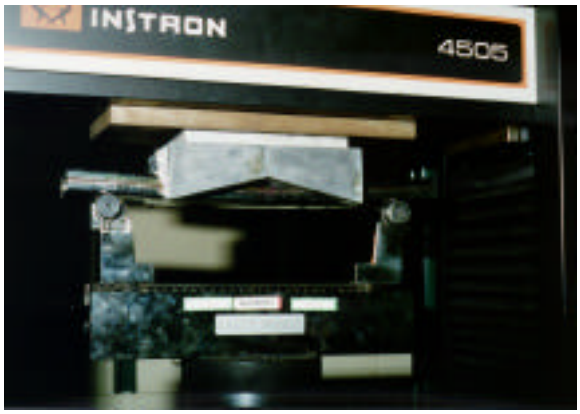

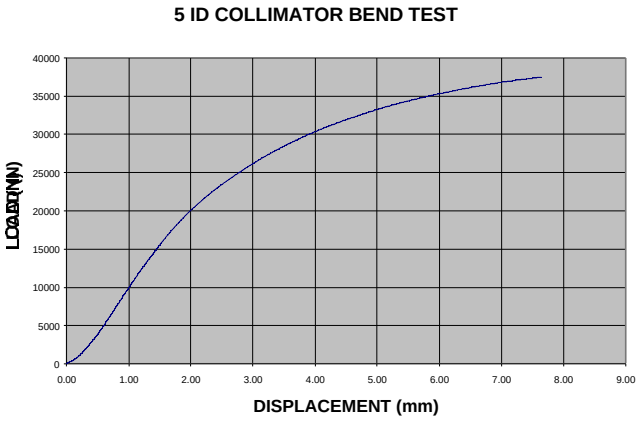

Fig. 5.11 Simulation of ratchet wall collimator distortion. (a) Bending test on the instron; (b) force deflection data.

activity and resulting corrosion inside the ratchet wall is a long-term concern. There are plans to evaluate this systematically during the next few years.

5.2.3 Beamline and Front-End Design for New Sectors and User Support

Front-End and Beamline Design for the SRI-CAT 1-ID Backscattering Beamline

The absence of beamlines in sectors 36 through 40 and the geometry of the components in the APS storage ring tunnel provide a unique opportunity to build a backscattering beamline on the 1-ID source. The concept for this unique capability was developed by David Moncton. The modifications required in the storage ring components to extract the x-ray beam have been completed by ASD. The front end and beamline have been designed for this 1-ID backscattering beamline. A redesign of the 1-ID front end has been completed so that there is minimal impact on SRI-CAT 1-ID beamline operation. Figure 5.12 shows plan and side views of the backscattering beamline layout. In scattering back from a yet-to-be-designed special monochromator in the 1-ID-B station, the beam penetrates the ring wall tangentially through a long vacuum transport. This specially designed 10-m-long vacuum pipe was procured and installed in the wall recently. The long pipe required a special support structure inside the shielding wall to optimize the alignment and positioning capability. These support pieces are manipulated for alignment from the end openings in the ring wall. Fig. 5.13 shows a photo of this support structure. In addition, a mono-beam shutter design, P8-50, has been completed for the 1-ID backscattering beamline, and backscattering monochromator design work is in progress to complete the beamline.

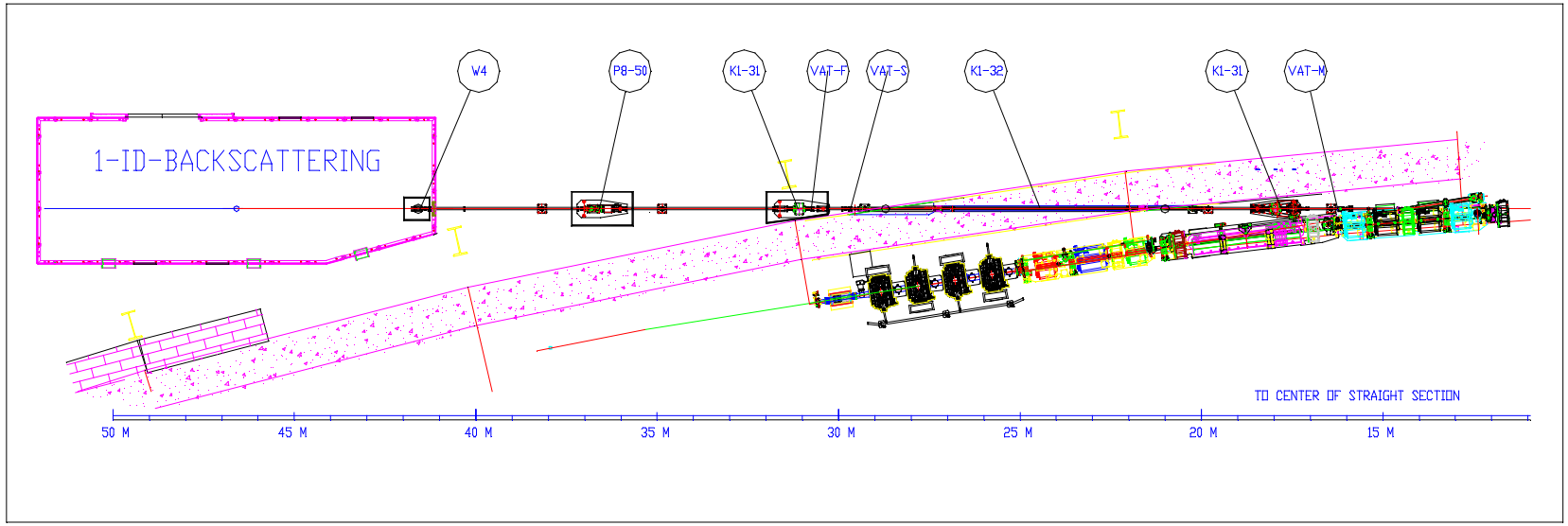

Fig. 5.12 Schematic layout of the 1-ID backscattering beamline. Beam enters from the right and travels to the left. W4: beryllium window, P8-50: monochromatic shutters, K1-31: collimator/differential pumps, VAT-F: fast valve, VAT-S: UHV valve, K1-32: 9-m wall collimator, VAT-M: all metal valve.

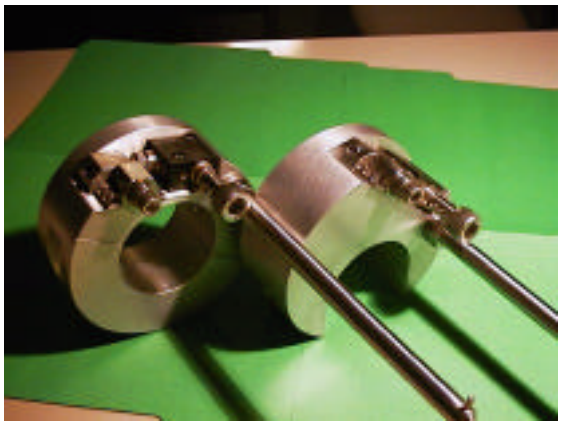

Fig. 5.13 Photo of the special support structure designed for the 10-m-long vacuum pipe in the 1-ID backscattering beamline.

SRI-CAT Sector 4 Beamline Design

A new sector was granted to SRI-CAT to develop techniques that use x-ray polarization for magnetic studies. The beamlines in this sector utilize unique undulators (see section 5.1.3) with radiation beams separated in the horizontal plane. The components for this set of beamlines on one straight section required special consideration. The design is now complete.

The front end for this beamline is shown in Fig. 5.14. All the 4-ID beamline front-end masks are designed for undulator A operated in the closed gap configuration at 130-mA stored current. Fixed mask M1-40 is made of a Glidcop® cylinder with stainless steel plates on both ends attached by explosive bonding. The first fixed mask of the 4-ID front end, M1-40, is 15.5 meters from the undulator A source. At 130-mA beam current and 11-mm gap, M1-40 will intercept an x-ray beam of 7.03-kW total power with 16.7-W/mm^2 peak power density (1.1^o incident angle). Thermal calculations using the ANSYS analytical package for the same operating conditions were carried out for the M1-40, M2-40, and M2-50 fixed masks, and the results are shown in Table 5.3.

A novel feature of this front end is the integrated design of the fixed mask and x-ray beam position monitor (XBPM) as a single unit. A chemical vapor deposition (CVD) diamond-based transmitting XBPM (Fig. 5.15) is mounted on the downstream side of the fixed mask. This new design not only reduces the front-end construction cost significantly but also improves the XBPM performance in rejecting the VUV and soft x-ray beam contamination. A prototype of this new design was tested at the APS 6-ID beamline FOE. Figure 5.16 shows the XBPM readout as a function of the beam vertical position.

Figure 5.17 shows the general layout of the sector 4 beamline branches. A total of six different fixed masks are being designed to allow the two undulators in the sector 4 straight section to be operated independently for two beamline branches. The experiment station design for SRI-CAT sector 4 is complete.

Table 5.3 Thermal calculations[a] for the M1-40, M2-40, and M2-50 fixed masks.

	M1-40	M2-40	M2-50
Distance from the Source (m)	15.5	16.2	20.0
Incident Angle (degrees)	1.1	1.1	1.4
Max. Power Density (W/mm^2)	16.7	15.2	12.8
Max. Temp. on Glidcopâ (°C)	255	267	260
Max. Temp. at Cooling Wall (°C)	98	100	102

[a] beam current = 130 mA, undulator gap = 11 mm

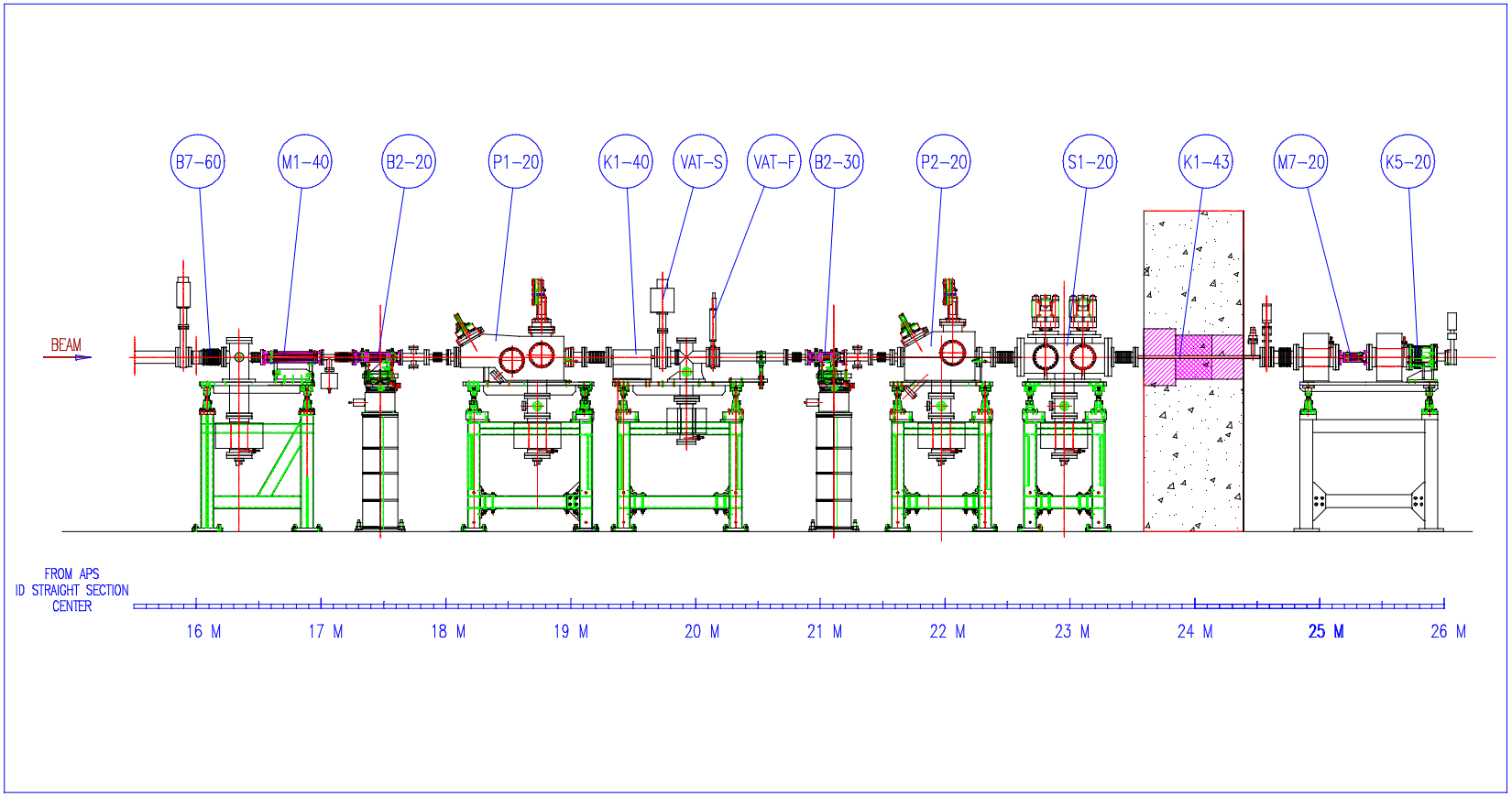

Fig. 5.14 Schematic layout of the 4-ID beamline front end. Beam enters from the left and travels to the right. B7-60: BM mask/bellows, M1-40: ID fixed mask, B2-20: first XBPM/fixed mask, P1-20: first photon shutter, K1-40: collimator, VAT-S: UHV valve, VAT-F: fast valve, B2-30: second XBPM/fixed mask, P2-20: second photon shutter, S1-20: safety shutter, K1-43: wall collimator, M7-20: fixed mask/differential pumps, K5-20: in-vacuum collimator.

Fig. 5.15 CVD-diamond-based transmitting XBPM, which is mounted on the downstream side of the fixed mask when installed on a beamline.

Beamline Components for CATs

Many beamline mechanical components have been designed and fabricated for many CATs. The ability to easily modify standard designs to meet unique goals and fabrication capabilities has generated such requests. The components in demand are slits (L5-90) and monchromatic beam shutters (P8-20). The CATs benefiting from this capability include COM-CAT, CHEMAT CARS, MU-CAT, and UNI-CAT, in addition to SRI-CAT.

Design Exchange

The XFD Design Exchange (DX) went through significant upgrading and

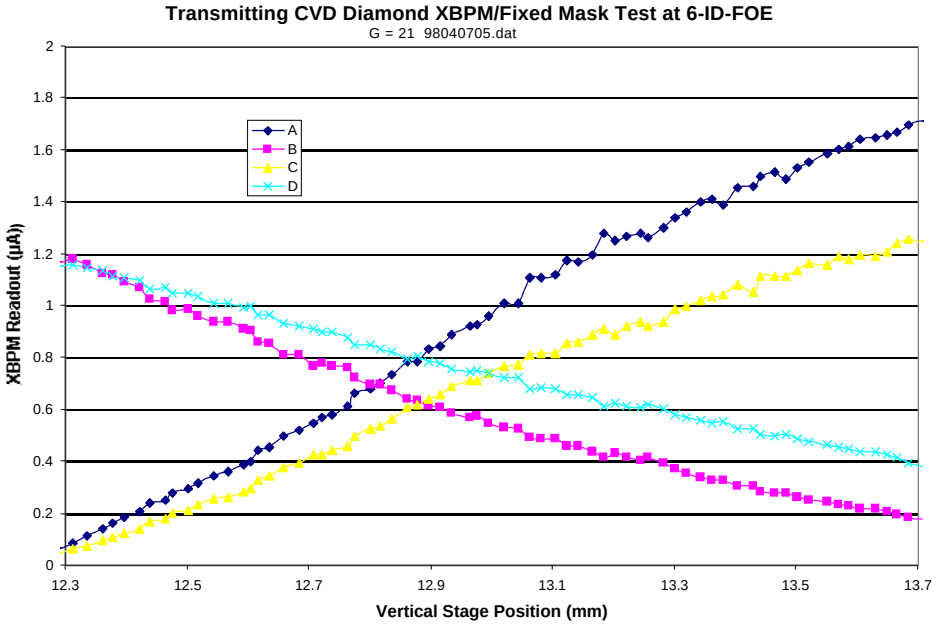

Fig. 5.16 The XBPM readout as a function of the beam vertical position.

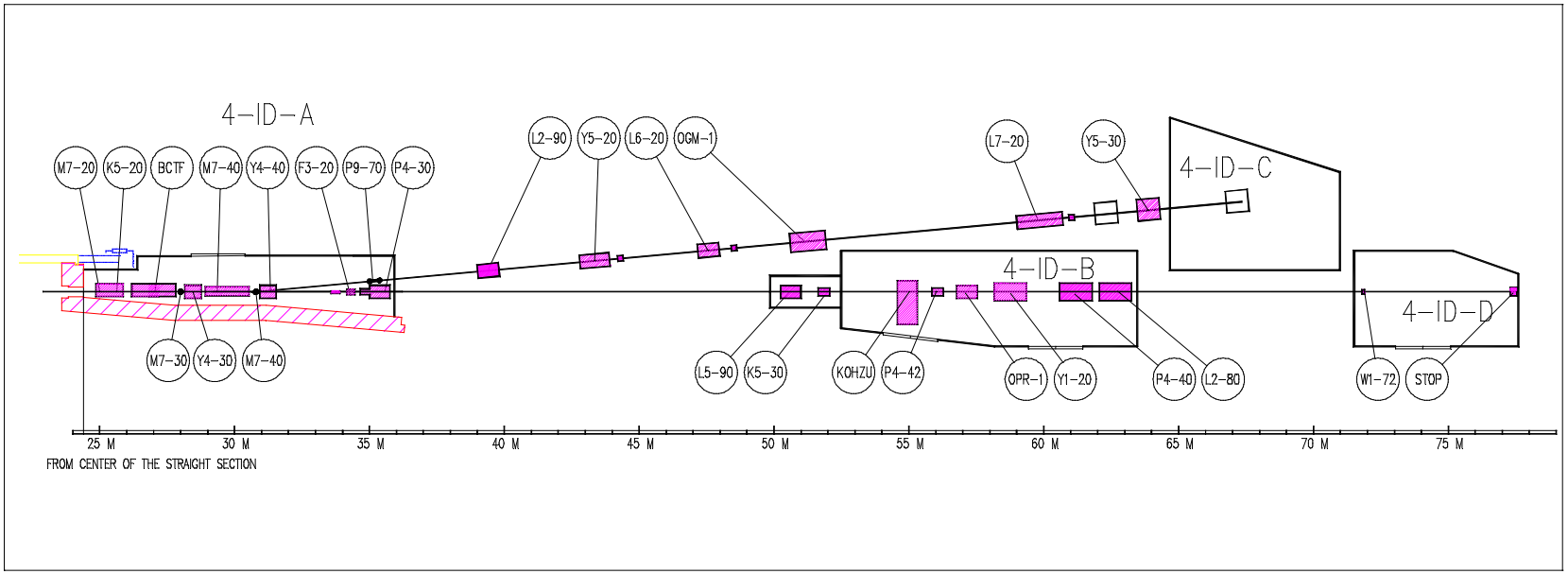

Fig. 5.17 Schematic layout of the sector 4 beamline capable of delivering two undulator beams simultaneously. Beam enters from the left and travels to the right. M7-20: fixed mask/differential pumps, K5-20: in-vacuum collimator, BCTF: beamline component test facility, M7-30: fixed mask plug, Y4-30: first horizontal mirror for station 4-ID-C, M7-40: dual-beam fixed mask, M7-50: fixed mask plug, Y4-40: second horizontal mirror for 4-ID-C, F3-20: filters, P9-70: pink-beam shutters, P4-30: white-beam integral shutters, L2-90: pink-beam slits/XBPM, Y5-20: first vertical mirror for 4-ID-C, L6-20: entrance slit, OGM-1: grating monochromator, L7-20: exit slit, Y5-30: refocusing mirror for 4-ID-C, L5-90: white-beam slits, K5-30: in-vacuum collimator, KOHZU: crystal monochromator, P4-42: white-beam stop, OPR-1: x-ray phase retarder, Y1-20: x-ray mirror, P4-40: white-beam integral shutters, L2-80: pink-beam slits, W1-72: beryllium window, STOP: beam stop.

renovation during the year. The following improvements were made in hardware and software.

We upgraded to Solaris 2.6 (Y2K compliant) and upgraded to a 22-GB hard drive for drawing storage; we are officially on R13 of AutoCad, supporting SAMBA services for file and print sharing. New Legato Networker Server software is now used to back up PCs, and work is still in progress on conversion from "A" numbers to "long filenames" for drawing libraries.

All design engineers and designers contributing to the DX are using Mechanical Desktop/AutoCAD 14. The PC stations available to mechanical engineers and design engineers were upgraded to meet the work requirements.

Scheduled backups take place on a regular basis for 60 PCs (out of 70 licenses available), and smooth and reliable storage, retrieval, and recovery of files are possible on server and workstations.

5.2.4 Laser Doppler Angular Encoder with Sub-Nanoradian Sensitivity

Recently, the demands for motion and control of optical elements increased. For example, in x-ray scattering experiments involving ultrahigh resolution (sub-meV at 10-30 keV), the motion control on the monochromating crystals has to be at the 1-to-10 nanoradian level or better (Toellner et al., 1997). However, if closed-loop feedback devices are used, the required resolution for the motion sensor (angular encoder) will be in sub-nanoradian level over a measuring range of 8 degrees.

There is, at present, no commercially available angular encoder with sub-nanoradian resolution over an 8-degree measuring range. In the field of grating-based encoders, one of the best available products is ROD-800 from Heidenhain, which has 175-nanoradian resolution with a 360-degree measuring range when coupled with an AWE 1024 interpolator (Heidenhain, 1996). As for commercial laser interferometers, the Hewlett Packard HP-5527B (Hewlett Packard, 1996) and Zygo ZMI-1000 (Zygo, 1996), provide a 20-100 nanoradian angular resolution from a few degrees up to 20 degrees angular measuring range. Although some tilt-sensors, such as the Applied Geomechanics Model-520, have 10-nanoradian resolution, they cover a measuring range of less than 0.01 degree with a very long measurement setting time (0.1-30 seconds).

In a laboratory setup based on a polarization-encoded Michelson interferometer system, a few nanoradian resolution has been achieved with a large setup (size about 610 mm × 1220 mm). A typical sine-bar configuration was used in this design to convert the angular measurement to a linear displacement measurement. The dimension of the sine bar was restricted to less than 310 mm in length by the monochromator structure and system stability limits. To achieve sub-nanoradian angular resolution, the resolution needed for the linear displacement measurement has to be in the near-Angstrom range. The overall dimensions of the encoder system are critical to the performance of the closed-loop feedback system. In general, however, the large setup size will cause complications for the system's thermal and mechanical stability.

The laser Doppler displacement meter (LDDM) is based on the principles of radar, the Doppler effect and optical heterodyning (Wang et al., 1987). We have chosen an LDDM as our basic system not only because of its high resolution (10 nm typical) and high measuring speed but also because of its unique performance—independent of polarization—which provides the convenience to create a novel multiple-reflection-based optical design to attain near-Angstrom linear resolution extension.

Figure 5.18 shows the self-aligning 3-D multiple-reflection optical design for the LDDM system resolution extension. In this design, the heterodyning detector is housed coaxially inside the frequency-stabilized laser source. Instead of a typical single reflection on the moving target, the laser beam is reflecting twenty-four times between the fixed base and the moving target. The laser beam, which is reflected back to the heterodyning detector, is frequency-shifted by the movement of the moving target relative to the fixed base. With same LDDM laser source and detector electronics, this optical path provides twelve-times resolution extension power for the linear displacement measurement and encoding. The 3-D optical path configuration results in a compact and integrated optical design that optimizes the system's antivibration performance, which is critical for sub-nanoradian resolution in measurements.

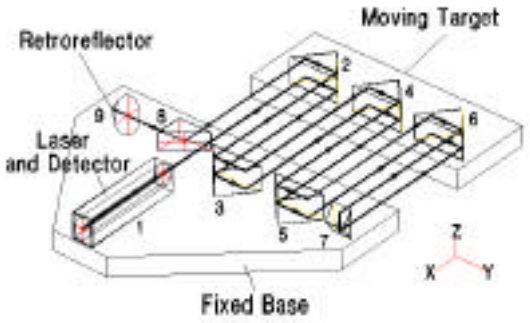

Fig. 5.18 The self-aligning 3-D multiple-reflection optical design for the LDDM system resolution extension.

Supported by a Laboratory Directed Research and Development (LDRD) award, a prototype laser Doppler angular encoder (LDAE) has been developed for high-energy-resolution x-ray scattering applications at the APS undulator beamline 3-ID. We have modified the monochromator (AAG-100, manufactured by Kohzu Seiki Co., Japan) sine bar and related structure for the LDAE assembly. Figure 5.19 shows the configuration of an actual LDAE system with twenty-four multiple-reflections on the one end of the sine bar, which rotates the shaft on which the asymmetrically cut

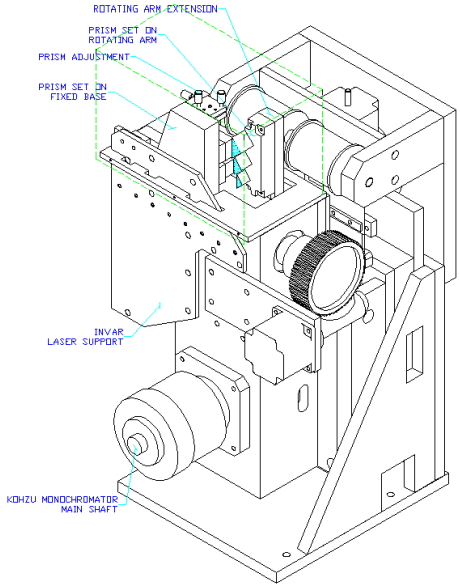

Fig. 5.19 Configuration of an actual LDAE system with twenty-four multiple-reflections on the one end of the sine bar, which rotates the shaft on which the asymmetrically cut crystals are mounted.

crystals are mounted. To control the system's thermal stability, a water-cooling jacket was attached to the laser source housing. Figure 5.20 shows a photograph of the monochromator with the LDAE.

Figure 5.21 is the plot of the test results that correlates the performance of our LDAE with a Heidenhain ROD-800 optical encoder with a 2-arc sec accuracy and 175-nanoradian resolution. The slope of the correlation data in Fig. 5.21 shows that our LDAE has a 0.2762 nanoradian per count readout sensitivity. A 100 mrad/sec rotation speed was tested for a laboratory setup in the 8-degree measuring range without any encoder miscounting.

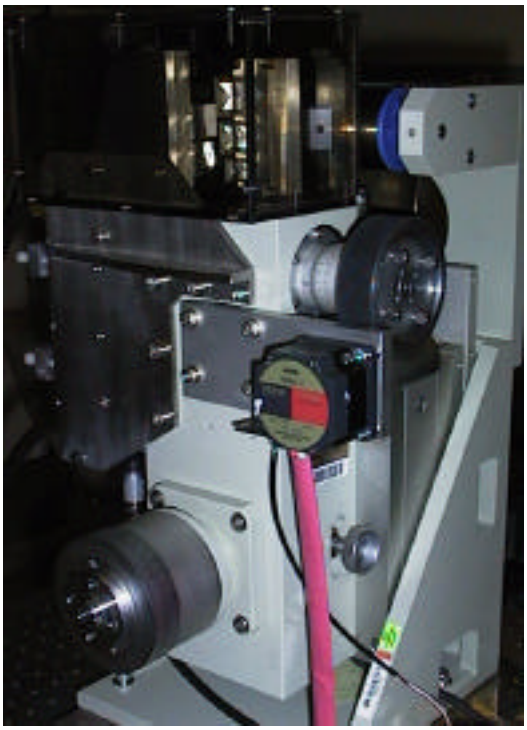

Fig. 5.20 Photograph of the monochromator with the LDAE.

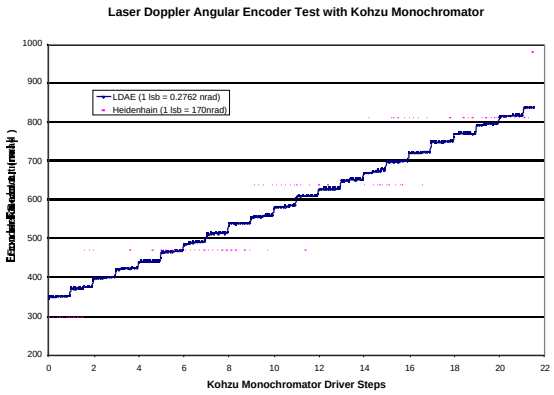

Fig. 5.21 Plot of the test results that correlates the performance of our LDAE with a Heidenhain ROD-800 optical encoder with a 2-arc sec accuracy and 175-nanoradian resolution.

It is very difficult to prove a sub-nanoradian system resolution experimentally in an open-loop system, because of the thermal and mechanical vibration noises. However, with a commercial piezoelectric transducer (PZT) driver, such as a Queensgate NPS3330, we have made an open-loop test with two 6.6-nanoradian motion steps. During this test, the same sine bar and the LDAE moving target were driven by a Queensgate PZT drive. Figure 5.22 is the plot of the test results that correlates the readout sensitivity with the Queensgate PZT driver with two 6.6-nanoradian jumps. The error bar on Figure 5.22 reflects the PZT driver system noise, which was about 1.9 nanoradians peak-to-peak. Recently, work has been initiated on a driving system with closed-loop configuration and 1-nanoradian resolution.

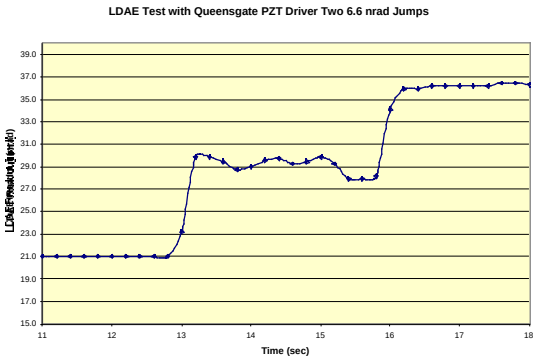

Fig. 5.22 Plot of the test results that correlates the readout sensitivity with the Queensgate PZT driver with two 6.6-nanoradian jumps.